Acta Astronautica 105 (2014) 285–297

Contents lists available at ScienceDirect

Acta Astronautica

journal homepage: www.elsevier.com/locate/actaastro

Longitude-dependent effects of fragmentation events in the geosynchronous orbit regime

Paul V. Anderson *, Hanspeter Schaub

Department of Aerospace Engineering Sciences, University of Colorado, 429 UCB, Boulder, CO 80309, USA

ARTICLE INFO

Article history:
Received 27 June 2014
Received in revised form
3 September 2014
Accepted 16 September 2014
Available online 28 September 2014

Keywords:
Geosynchronous orbit
Orbital debris
Fragmentation events

ABSTRACT

The effects of on-orbit fragmentation events on localized debris congestion in each of the longitude slots of the geosynchronous orbit (GEO) regime are evaluated by simulating explosions and collisions of uncontrolled rocket bodies in multiple orbit configurations, including libration about one or both of the gravitational wells located at 75°E and 105°W. Fragmentation distributions are generated with the NASA Standard Breakup Model, which samples fragment area-to-mass ratio and delta-velocity as a function of effective diameter. Simulation results indicate that the long-term severity and consequence of a GEO fragmentation event is strongly dependent upon parent body longitude at the epoch of fragmentation, which can spawn bi-annual "fragment storms" in high-risk longitude slots, driven by lower-energy fragments that have been captured and have started librating around the nearby gravitational well.

1. Introduction

The geosynchronous orbit (GEO) regime is a unique commodity of the Earth-orbiting satellite industry that is becoming increasingly contaminated with orbital debris [15,14], but is heavily populated with high-value assets [7]. As the lack of environmental cleansing mechanisms at the GEO altitude renders the lifetimes of orbital debris in this regime essentially infinitely long, conjunction assessment must be performed to safeguard operational assets from potential collisions with the debris population in GEO, which could have costly financial, legal, and geopolitical consequences. GEO satellites are required to maintain a specified longitude slot, and cannot simply phase shift in true anomaly to evade debris. Thus, analyses of the macroscopic behavior of the debris population at GEO are useful for describing debris fluxes through particular GEO longitude slots, to forecast how often operators with expensive assets in these regions must perform conjunction assessment and potentially execute dedicated maneuvers to evade uncontrolled debris objects.

Of critical importance is a thorough understanding of the consequences that on-orbit explosions and debris–debris/debris–asset collisions, collectively classified as *fragmentation events*, have on longitude-dependent congestion throughout the GEO regime. This knowledge is especially relevant, since although two historical fragmentation events at GEO have been documented—the 1978 explosion of the Ekran-2 payload, and the 1992 explosion of a Titan III-C transtage [19]—significant populations of objects with diameters as small as 10–15 cm have been detected in optical observations of the GEO ring, and are indicative of undocumented fragmentation events in this regime [19,27,26]. Although no known historical collision events have been documented at GEO, potential impact-induced anomalies have been observed in both the GEO ring and the super-synchronous GEO graveyard regime [23]. Fragmentation on-orbit is triggered by

* Corresponding author.
E-mail addresses: paul.anderson@colorado.edu (P.V. Anderson), hanspeter.schaub@colorado.edu (H. Schaub).

http://dx.doi.org/10.1016/j.actaastro.2014.09.011
0094-5765/

accidental mixing of hypergolic fuels, overheating of residual (non-vented) propellants, mechanical valve failures, hypervelocity impact, or other unknown/unattributed means [21].

Although the literature strongly focuses on the effects of debris-generating fragmentation events in low-Earth orbit (LEO), several previous studies have been devoted to quantifying increases in collision risk driven by fragmentations in the GEO ring. Yasaka and Ishii [32] utilize momentum and energy principles to model hypervelocity impacts and predict that the resulting fragment cloud remains close to the GEO altitude, and spreads longitudinally to all regions of the GEO ring within weeks. Oltrogge and Finkleman [25] consider a probable conjunction scenario at GEO to show that the fragment energy distribution resulting from breakup is sufficient for permeating all orbit regimes from re-entry through super-synchronous. Recently, Hansen and Sorge [11] indicate that although close approach velocities for the GEO regime are in general lower than in the LEO arena, a low-energy breakup over one of the gravitational wells could be a worst-case scenario in that resonance is preserved for most of the fragment population, serving to increase collision risk with operational assets at these longitudes. While the tools that the authors of these previous studies harness for characterizing breakup events at GEO differ, the independent conclusions of each study agree that fragmentations at the GEO altitude have long-term consequences that are detrimental to the sustainability and continuing usefulness of this orbit regime. Furthermore, in addition to these environmental consequences, a GEO fragmentation event and the effects thereof can hinder the high-value services of operational assets and engender political repercussions as well [25].

Forecasting of longitude-dependent congestion—termed "debris weather"—is an imperative for space situational awareness activities in the GEO regime, as it provides a metric to gauge how often operators with assets in particular longitude slots will have to track nearby debris motion and consider executing dedicated debris avoidance or multi-purpose maneuvers. Following a congestion metric proposed by Anderson and Schaub [2], this study harnesses a toroidal cell configuration at the GEO altitude to investigate localized effects of a variety of simulated fragmentation events in the GEO ring. Fragmentation particles are generated with the NASA Standard Breakup Model as presented in Johnson et al. [16], which has been validated against catalogued debris clouds and ground-based experimental results for particles larger than 1 mm [19]. This empirical model statistically samples fragment area-to-mass ratio and corresponding delta-velocity imparted to each particle at the fragmentation epoch, which is applied along a randomly sampled unit vector and added to the parent body's velocity vector. The congestion metric is employed with a parallel propagation routine that implements 4×4 EGM-96 gravitation, luni-solar perturbations, and the cannonball solar radiation pressure (SRP) model, to propagate fragments forward in time and assess the longitude-dependent congestion resulting from the simulated fragmentation.

It is imperative to determine whether the longitude of the parent body at the fragmentation epoch renders the localized effects of the break-up more or less severe for operational assets in higher-risk longitude slots, especially those in the vicinity of the gravitational wells at 75°E and 105°W. As will be demonstrated, on-orbit fragmentation in the GEO ring has the potential to generate significant localized congestion, dependent on both the longitude and altitude at which the fragmentation occurs. This paper thus fills a critical void in the literature by addressing fragmentation events at GEO from the perspective of the Earth-fixed frame, and not inertial space, which has typically been used for fragmentation studies in both the LEO and GEO regimes (e.g., [32,25]). On-orbit fragmentation for a variety of different break-up scenarios is simulated to rapidly investigate short- and long-term contributions to nominal, baseline congestion occurring on a localized basis for each of the GEO longitude slots. As the debris population continues to increase—especially as a result of fragmentation events—the amount of propellant required to maintain a specified longitude slot while simultaneously executing avoidance maneuvers, and the costs associated with reviewing conjunctions to determine if evasive action is even warranted, will begin increasing in tandem. From the new perspectives of this paper, the significance and implications of on-orbit fragmentations at GEO will be cast in a new light to impel further research in this critical area.

2. Methodology for forecasting localized congestion

2.1. Overview of near-miss events metric

Near-miss events for the GEO longitude slots are determined by formulating a GEO-encompassing torus of major radius $r_{\text{GEO}} = 42164$ km and minor radius $\tilde{r}$, partitioned into longitude increments of $\Delta\lambda = 1.0^\circ$ [2]. The minor radius $\tilde{r}$ is equivalent to the radius of the circular torus cross-section, and provides a means to evaluate debris congestion levels occurring within various distances of the GEO longitude slots, i.e., a larger minor radius captures more near-miss events. In this study, a representative minor radius of $\tilde{r} = 100$ km is considered, as this radius provides a conservative upper bound for distances at which precise conjunction assessment could potentially be considered for operational GEO satellites. Furthermore, this torus formulation is a natural choice for detecting near-miss events for the non-inertial longitude slots, as torus geometry is invariant as seen by both the Earth-centered inertial frame and the Earth-centered, Earth-fixed frame, in which the GEO longitude slots are stationary [2].

Near-miss events are detected during propagation of an object by checking for transversal of this GEO torus boundary at each time step during numerical integration. If finer resolution is desired, an interpolation method can be implemented to check for torus intersections between integration time steps. Mathematically, a near-miss event occurs if [2]

$$\left(r_{\text{GEO}} - \sqrt{r_X^2 + r_Y^2}\right)^2 + r_Z^2 - \tilde{r}^2 < 0 \tag{1}$$

is satisfied, where $(r_X, r_Y, r_Z)^T$ is the RSO position vector expressed in inertial frame components. The longitude of intersection λ_{CPE} is determined as

$$\lambda_{\text{CPE}} = \arctan\left(\frac{r_Y}{r_X}\right) - \alpha_G \tag{2}$$

where α_G is the right ascension of Greenwich (Greenwich sidereal time) [8]. When a torus intersection is detected with

Eq. (1), the longitude of intersection is determined with Eq. (2), and the total near-miss event count for the associated torus cell is updated. To ensure that equivalent intersections are not accounted for more than once during event checking, counting logic is implemented before a cell intersection counter is updated to screen the event for redundancy. The full algorithm for quantifying GEO debris congestion with the GEO torus formulation and near-miss event metric is detailed in Anderson and Schaub [2].

2.2. Propagator and implementation

A special perturbations propagation routine implemented in ANSI-C and parallelized with OpenCL is used to propagate fragments forward in time and determine torus intersection events.[1] Specifically, the two-body equations of motion are numerically integrated under 4×4 EGM-96 gravitation, luni-solar perturbations, and the solar radiation pressure (SRP) effect, modeled with the "cannonball" approximation described by Vallado [29], and attenuated by the occultation algorithm presented by Montenbruck and Gill [24]. This lower-fidelity, representative GEO force model yields dramatically decreased simulation run times while resulting in negligible congestion differences with higher-fidelity force model simulations. The equations of motion are

$$\ddot{\boldsymbol{r}} = -\frac{\mu_\oplus}{r^3}\boldsymbol{r} + \boldsymbol{a}_\oplus + \boldsymbol{a}_\leftmoon + \boldsymbol{a}_\odot + \boldsymbol{a}_{\mathrm{SRP}} \tag{3}$$

where the first term denotes two-body acceleration, $\boldsymbol{a}_\oplus$ is the acceleration due to the nonsphericity of Earth, $\boldsymbol{a}_\leftmoon$ and $\boldsymbol{a}_\odot$ are the third-body perturbations from the Moon and Sun, respectively, and $\boldsymbol{a}_{\mathrm{SRP}}$ is the SRP acceleration. SRP is modeled using the inverse-square diffusion formulation of the solar luminosity $L_\odot \approx 3.839 \times 10^{26}$ J/s, with coefficient of reflectivity $c_r \equiv 1.5$ and area-to-mass ratio $A_\odot/m$ sampled in the NASA Standard Breakup Model, as discussed in Section 2.3. This force model is in agreement with the results of Hansen and Sorge [11], who rank the importance of incorporating various environmental perturbations in GEO force models for debris analysis over time scales ranging from 1 week to 10 years. This study treats fragmentation-induced congestion over a minimum 5-year duration, a time scale over which luni-solar perturbations become especially relevant for uncontrolled debris at GEO.

In higher-fidelity force models, coordinate transformations between Earth-fixed and Earth-inertial frames utilize accurate Earth orientation parameters to account for precession, nutation, and polar motion—software suites such as the SPICE toolkit can be harnessed to perform these complex coordinate transformations.[2] In this parallelized propagator, however, a lower-fidelity transformation that accounts strictly for a z-axis rotation by Greenwich sidereal time is used for purposes of increased speed at run time. Furthermore, instead of extracting Moon/Sun position vectors from the DE-421 ephemerides, this routine implements low-precision formulae for the geocentric coordinates of these bodies, as provided in the 2013 *Astronomical Almanac* [28]. Anderson and Schaub [3] validate this lower-fidelity force model by comparing the congestion results over a five-year period with those obtained using a higher-fidelity force model. Since debris congestion trends equivalent to those presented in the current paper change insignificantly when higher-fidelity forcing is used, lower-fidelity, parallel propagation is harnessed for the dramatic speed increase it provides.

The propagator utilizes an eighth-order, predictor–corrector Gauss–Jackson integrator [4] initialized with the Prince–Dormand 8(7) algorithm for integrating the equations of motion in Eq. (3). For near-miss event detection during the congestion forecast, a time step of 1 min is specified for sufficient fidelity in capturing macroscopic congestion trends. To enhance resolution without significantly increasing run times, linear interpolation is used to check for torus intersections in 6 s increments between primary time steps. Linear interpolation is an appropriate assumption in this case, because an object in a two-body GEO orbit will move through a circular arc of $\theta_{\mathrm{arc}} \approx 0.25^\circ$ in one time step. At the GEO altitude, the straight-line approximation over this time step will only deviate from the true curvilinear orbit by approximately $r_{\mathrm{GEO}}[1-\cos(\theta_{\mathrm{arc}}/2)] \approx 0.1$ km at maximum, based on the geometry of circular segments. Since the GEO torus cells considered for this study have a minor radius of 100 km, this discrepancy of 0.1 km does not significantly affect the resolution of the resulting congestion forecast.

2.3. Fragmentation model

In this study, fragmentation particles are generated using the NASA Standard Breakup Model, developed for NASA's long-term debris environment software EVOLVE 4.0 [16] and validated against catalogued debris clouds and ground-based experimental results for particles larger than 1 mm [19]. This model uses an empirical power law to determine the cumulative number of fragments larger than a user-defined effective diameter l_c. For explosions, the cumulative number of fragments N_f is independent of the mass of the parent body, and is given by

$$N_f(d \geq l_c) = 6 c_s l_c^{-1.6} \tag{4}$$

where d denotes fragment diameter, l_c the effective diameter defined in units of meters, and c_s a unitless, empirical correction for catalogued fragmentation events [19]. For this study, the correction $c_s = 1.0$ is assumed.[3] For collisions, N_f is a function of the target and impactor masses and collision velocity [19]:

$$N_f(d \geq l_c) = 0.1 \hat{m}^{0.75} l_c^{-1.71} \tag{5}$$

[1] *OpenCL 1.2 Specification* is available from Khronos Group at: http://www.khronos.org/registry/cl/.

[2] NASA/JPL's SPICE toolkits are available at: http://naif.jpl.nasa.gov/naif/toolkit.html.

[3] Johnson et al. [16] indicate this relationship is valid for launch vehicle upper stages with mass 600–1000 kg, and introduce the correction factor c_s to account for known debris from catalogued explosions of other parent body masses and types.

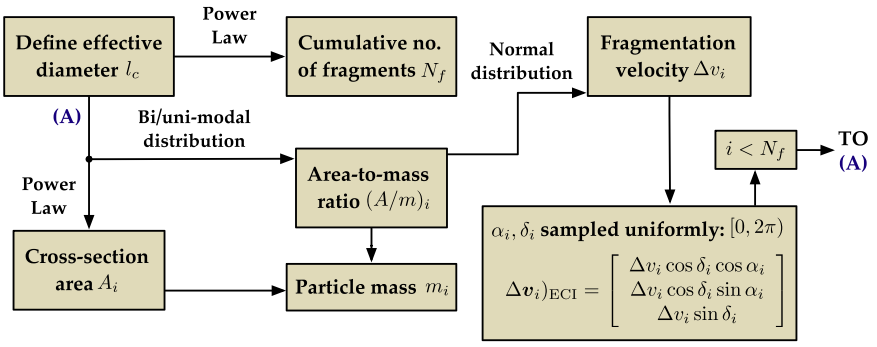

Fig. 1. Flow-chart for computer implementation of the NASA Standard Breakup Model.

where the mass-dependent factor $\hat{m}$ is defined as

$$\hat{m} \equiv \begin{cases} m_t + m_p \text{ [kg]} & \text{for } \tilde{E}_p \geq \tilde{E}_p^* \quad \text{[catastrophic]} \\ (m_p v_i)/1000 \text{ [kg m/s]} & \text{for } \tilde{E}_p < \tilde{E}_p^* \quad \text{[non−catastrophic]} \end{cases} \tag{6}$$

where m_t and m_p denote target and impactor masses, v_i is the impact speed, $\tilde{E}_p = 0.5 m_p v_i^2 / m_t$ is the specific energy of the impactor, and $\tilde{E}_p^* \equiv 40$ kJ/kg is the energy threshold for a catastrophic collision [19]. For effective diameters $l_c > 11$ cm, a bi-modal probability distribution is used to sample the area-to-mass ratio for every fragment. For $l_c < 8.0$ cm for spacecraft fragments, and $l_c < 1.7$ cm for upper stage fragments, a single-mode normal distribution is employed [19]. For effective diameters in the definition gap of 8–11 cm for spacecraft and 1.7–11 cm for upper stages, a pseudo-random number on [0,1] is generated to determine if the bi-modal or single-mode distribution should be employed [19]. The cross-sectional area for each fragment is then determined as an explicit function of the effective diameter l_c, and the fragmentation delta-velocity Δv_i applied to each fragment is sampled from a normal distribution on the area-to-mass ratio [16]. Fig. 1 provides a flow-chart for using the NASA model—for more details regarding implementation, and for the parameters input into the bi-modal and single-mode area-to-mass ratio and delta-velocity distributions in the model, see Johnson et al. [16] and Klinkrad [19].

Note that for both explosion and collision events, the delta-velocity Δv_i is applied in a random direction sampled over the unit sphere for each fragment. For this study, right ascension and declination angles are sampled uniformly over the unit circle, and these angles are translated into a unit vector direction with spherical coordinates (cf. Fig. 1). Note that the resulting unit vector distribution is not uniform—rather, it exhibits slight bias towards the poles.[4] In the event of a collision, the number of fragments in each generated debris cloud is proportional to the mass fractions of the target and impactor, e.g., the target cloud receives $[m_t/(m_t+m_p)]N_f$ fragments, and the impactor cloud $[m_p/(m_t+m_p)]N_f$ fragments, such that each cloud receives $0.5N_f$ fragments inasmuch as $m_t = m_p$. Since the objective of this study is to investigate the longitude-dependent effects of fragmentations at GEO—and not the accuracy of the fragmentation model itself—these assumptions are appropriate for this study.

Table 1
Orbit classifications for geosynchronous objects used in GEO congestion study.

Class	Type	Description
C1	Controlled	Longitude/inclination control (E–W/N–S control)
C2	Controlled	Longitude control only (E–W control only)
D	Drifting	Drift above/below/through protected GEO zone
L1	Librating	Libration about Eastern stable point ($\lambda = 75°$E)
L2	Librating	Libration about Western stable point ($\lambda = 105°$W)
L3	Librating	Libration about Eastern/Western stable points
IN	Indeterminate	Unknown status (e.g., recent TLE not available)

3. Background noise from current debris population

The resident space object (RSO) population in the GEO regime is classified with a taxonomy used by the European Space Agency's DISCOS database (Database and Information System Characterising Objects in Space) [9]. For GEO objects, seven orbit categories are selected to classify the type of orbits traversed by these objects. Table 1 gives a description of this classification system; only uncontrolled objects are assumed to contribute to localized congestion in this study. GEO objects are selected according to the requirements imposed in ESA's annual *Classification of Geosynchronous Objects* reports [9]:

- Eccentricity smaller than 0.2 ($e < 0.2$).
- Inclination smaller than 70° ($i < 70°$).
- Mean motion between 0.9 and 1.1 revolutions per sidereal day ($0.9 < n < 1.1$).[5]

[4] Though the direction of the delta-velocity vector is central to the instantaneous change in orbital elements experienced during fragmentation, it is ultimately the coupling between magnitude and direction that determines if a fragment will librate around a gravitational well. Thus, this non-uniform vector distribution is sufficient for the purposes of this study.

[5] This mean motion range corresponds to the semi-major axis range $[-2596, 3068]$ km with respect to the GEO radius.

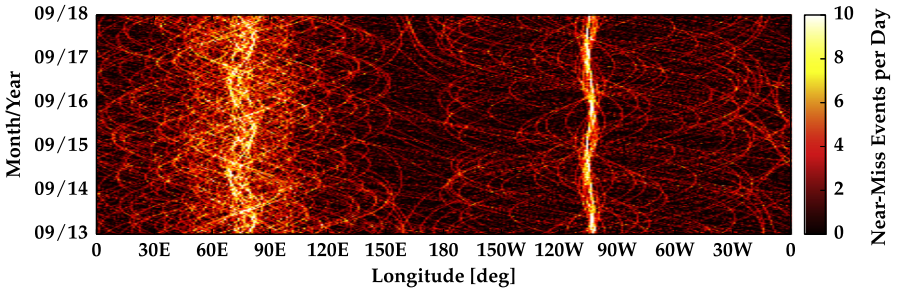

Fig. 2. Five-year localized debris congestion forecast at GEO (100 km torus).

Orbital data are obtained from publicly available two-line element (TLE) sets provided by U.S. Strategic Command (USSTRATCOM).[6] For this study, a reference TLE set obtained on 08/28/2013 is used. TLE data are given in the form of doubly averaged Keplerian elements with mean motion instead of semi-major axis [19], transformed into Cartesian states cast in the true equator, mean equinox (TEME) frame [29] using SGP-4 theory [13].[7] Note that because of the limited accuracy of the TLE sets, these data are not intended for studies that require highly precise orbit prediction capabilities. As the purpose of this paper is to forecast localized debris congestion generated from on-orbit fragmentation events on a macroscopic scale, the accuracy of these data is sufficient for this baseline "background noise" assessment. Furthermore, as only objects larger than approximately 0.8–1.0 m in effective diameter are actively tracked at the GEO altitude [9], only objects at least of this size are considered in the background noise forecast.

As a precursor to identifying the longitude-dependent effects of fragmentations at GEO, a 5-year macroscopic congestion forecast is performed with the minor radius $\tilde{r} = 100$ km, using the GEO debris population in the 08/28/2013 TLE data set to evaluate current levels of background noise in this ring. Controlled satellites (C1/C2) are assumed to maintain their designated longitude slots, while the 750 uncontrolled GEO objects in this set are propagated forward in time and incorporated in the congestion forecast. Note that this simulation only assesses the congestion derived from the current debris population over a 5-year time frame. Nominal population growth,[8] solid rocket motor (SRM) slag, multi-layered insulation (MLI) shedding, and other debris growth mechanisms considered in Wegener et al. [31], for example, are not treated here.

The localized congestion forecast for GEO over this 5-year period is shown in Fig. 2, which illustrates the number of near-miss events at 100 km per day for each of the GEO longitude slots. Accumulation of uncontrolled objects around the gravitational wells at 75°E and 105°W is a well-known result, as is discussed by Luu and Sabol [20] and Chobotov [6]. This is a particularly troublesome notion, as operational assets are typically inserted into longitude slots near the gravitational wells [3], and the annual probability of collision in the vicinity of these gravitational wells is an estimated seven times higher than in surrounding regions at GEO [7,22]. From Fig. 2, controlled satellites in the longitude slots neighboring the gravitational wells are subject to 6–10 near-miss events per day at a distance of 100 km—this is on-par with the factor of seven increase over less congested longitude slots that experience a maximum of 1–2 near-misses per day at 100 km (e.g., over the Atlantic and Pacific Oceans). It is critical to emphasize that even though this increase in near-miss events around the gravitational wells is comparable to the increase in probability of collision in these regions, the number of near-miss events for a given longitude slot over any time frame is not equivalent to any form of the probability of collision measure used for operational conjunction assessment. Again, since this congestion forecast only includes the trackable, catalogued, and unclassified GEO derelicts with up-to-date TLE data, these results serve to illustrate a conservative lower bound of the actual debris background noise in the GEO ring.

4. Longitude-dependent effects of fragmentations at GEO

The longitude-dependent congestion generated by fragmentation of a rocket body (R/B) over one of the gravitational wells at 75°E and 105°W is characterized by applying the NASA Standard Breakup Model to a simulated R/B positioned in various longitude slots at GEO. Hansen and Sorge [11] hypothesize that a lower-energy fragmentation over one of the gravitational wells could be a worst-case scenario in that resonance is preserved for a majority of the fragments generated by the fragmentation, resulting in frequent near-misses with operational assets in the vicinity of these critical longitudes. The results of this current study will illustrate that this hypothesis of Hansen and Sorge [11] is exactly the case—not only does longitude-dependent congestion increase as a function of the number of fragments captured by the gravitational well, but these localized congestion increases are predictable to first-order both in longitude and time since fragmentation. First, we examine theory introduced by Allan [1], who provides the mathematics necessary for predicting libration parameters based upon initial longitude and longitudinal drift rate $\dot{\lambda}$. These parameters are combined with a harmonic oscillator model to provide a first-order, analytic formulation for the resulting libration motion of fragments captured by a gravitational well.

[6] Publicly available TLE data sets are available for bulk download from https://www.space-track.org/.

[7] ANSI-C implementation of merged SGP-4/SDP-4 theory is available from http://www.sat.dundee.ac.uk/~psc/sgp4.html [30].

[8] The effect of nominal launch traffic on longitude-dependent debris congestion at GEO is studied by Anderson and Schaub [3].

4.1. Harmonic oscillator model of libration motion

Using a change of origin $\psi \equiv \lambda - \lambda_{1,2}$, where λ and $\lambda_{1,2}$ denote geocentric longitude of the object and gravitational well, respectively, the condition for stable point "capture" is expressed as [1]

$$\|\dot{\psi}_0\| < k\|\cos\ \psi_0\| \tag{7}$$

where $\dot{\psi}_0 = n_0 - n_{\mathrm{GEO}}$ is the initial longitudinal drift rate (a function of the semi-major axis only), and k is an angular-velocity-like parameter dependent upon the $J_{2,2}$ sectorial harmonic and defined as [1]

$$k \equiv \frac{6 n_{\mathrm{GEO}} R_{\oplus} \sqrt{J_{2,2}}}{r_{\mathrm{GEO}}} \tag{8}$$

Utilizing the coefficient $J_{2,2} \approx 1.82 \times 10^{-6}$ derived from the EGM-96 gravity model,[9] the parameter $k \approx 8.92 \times 10^{-8}$ rad/s [19]. Following Allan [1], the amplitude and period of libration for objects that satisfy the capture condition in Eq. (7) are approximated by the two formulas:

$$\sin\ \psi_m = \sqrt{\sin^2 \psi_0 + \frac{\dot{\psi}_0^2}{k^2}} \tag{9}$$

$$T_l = \frac{4}{k} K(\sin\ \psi_m) \tag{10}$$

where ψ_m denotes the libration amplitude, T_l is the period of libration, and $K(\sin\ \psi_m)$ is the complete elliptic integral of the first kind [1]. Note that Eqs. (9) and (10) are derived assuming the $J_{2,2}$ term only; higher-order harmonics appearing in a full expansion of the Earth gravitational potential are neglected. Therefore, since the propagator harnessed in this study uses a 4×4 gravitation model, Eqs. (9) and (10) provide a first-order approximation for the libration characteristics observed with numerical simulations. Nonetheless, these formulas can be used in tandem with a harmonic oscillator model to rapidly predict libration motion to first-order, i.e., under the $J_{2,2}$ perturbation alone. If oscillatory motion is assumed, the longitudinal motion of a captured object can be expressed as

$$\lambda(t) = \psi_m\ \cos\left(\frac{2\pi t}{T_l} - \phi\ \mathrm{sgn}(\dot{\psi}_0)\right) + \lambda_{1,2} \tag{11}$$

where the phase shift ϕ is determined with

$$\phi = \arccos\left(\frac{\psi_0}{\psi_m}\right) \tag{12}$$

Note that the sign of the initial longitudinal drift rate $\dot{\psi}_0$ is included to switch the sign of the phase angle accordingly, such that the resulting sinusoidal longitude profile reflects the initial East/West drifting direction of the object. The accuracy of this harmonic oscillator model for predicting resulting libration motion of fragments captured by a gravitational well in the aftermath of fragmentation is explored in Section 4.2, which simulates explosions in the neighborhoods of the critical stable points.

[9] Coefficients for the EGM-96 model are available at: http://cddis.nasa.gov/926/egm96/egm96.html.

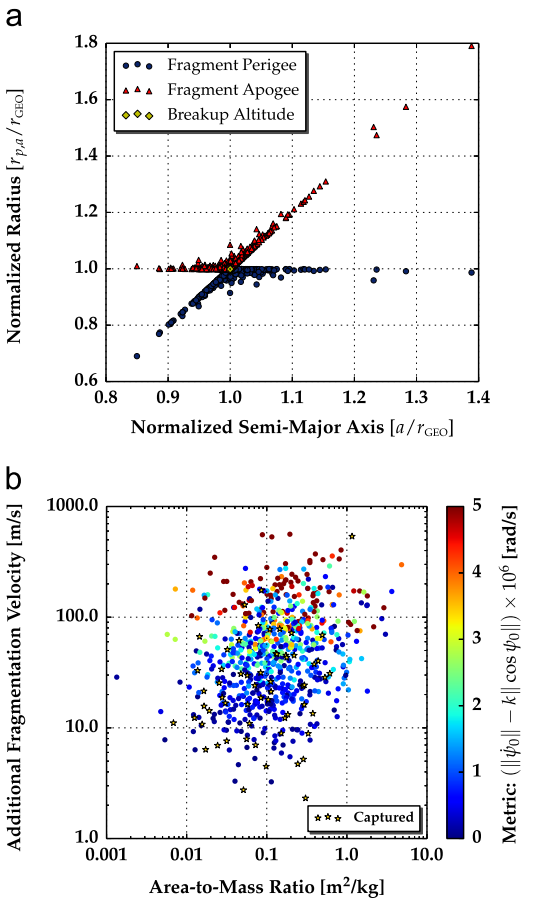

Fig. 3. Characteristics of fragmentation distribution for simulated explosion at 60°E. (a) Gabbard diagram for R/B explosion at 60°E and (b) fragment distribution for R/B explosion at 60°E.

4.2. Rocket body explosions over gravitational wells

To investigate longitude-dependent debris congestion generated by explosions at the GEO altitude, the NASA Standard Breakup Model is applied to generate fragmentation debris with effective diameters $l_c > 5$ cm resulting from the explosion of a simulated R/B, with initial conditions that place the R/B at various longitudes surrounding the Eastern/Western gravitational wells at the simulated explosion epoch of midnight on 09/01/2013. From Eq. (4), the NASA model predicts that 724 fragments larger than 5 cm are generated in the explosion. The fragmentation delta-velocity for each fragment is applied in a random direction sampled over the unit sphere, and is added to the inertial velocity vector of the simulated R/B initial conditions $a = r_{\mathrm{GEO}}$, $e = 0.001$, $i = \Omega = M_0 = 0°$, with the argument of perigee ω chosen such that the R/B is positioned at the desired longitude, i.e., $\omega = \alpha_G + \lambda_0$, where α_G is the right ascension of Greenwich at the explosion epoch [3].

Fig. 3 provides the characteristics of the resulting fragment distribution for the case $\lambda_0 = 60°$E. Fig. 3(a) shows a Gabbard diagram that highlights the resulting perigee/apogee radius spread as a function of semi-major axis, normalized by the GEO radius, and Fig. 3(b) shows the area-to-mass ratio and

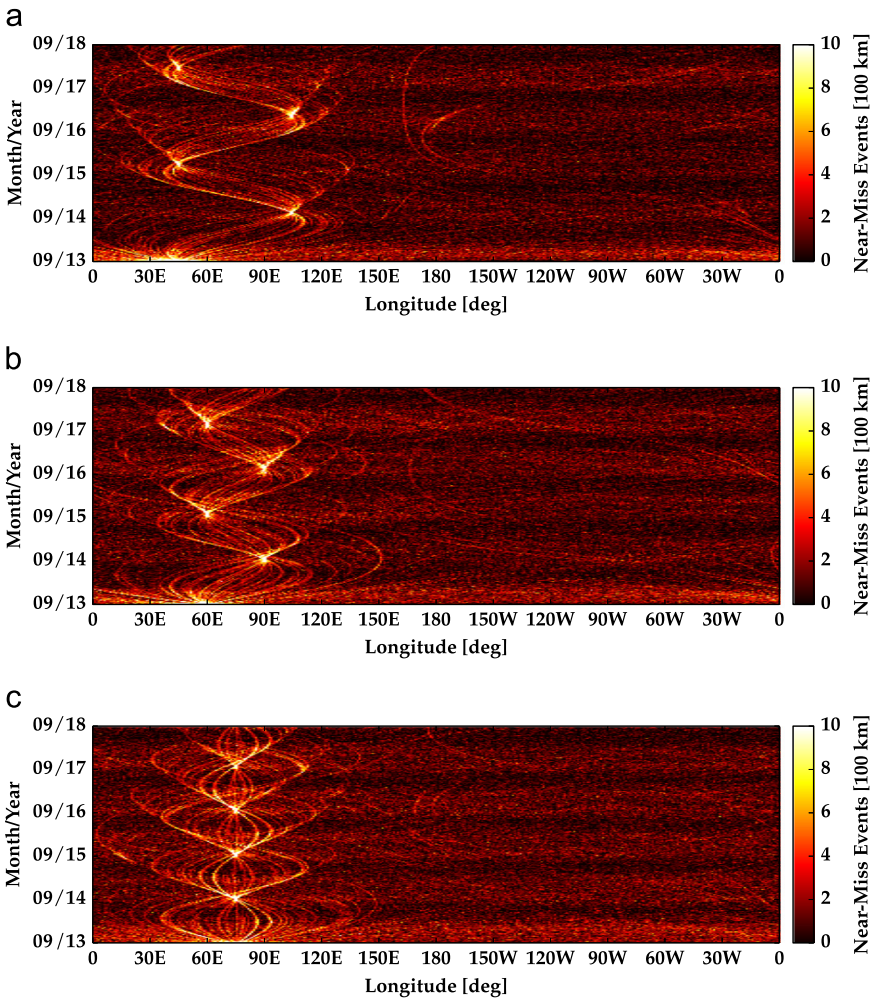

Fig. 4. Longitude-dependent congestion from simulated R/B explosions by Eastern well. (a) Five-year congestion forecast for simulated explosion at 45°E ($\tilde{r} = 100$ km). (b) Five-year congestion forecast for simulated explosion at 60°E ($\tilde{r} = 100$ km). (c) Five-year congestion forecast for simulated explosion at 75°E ($\tilde{r} = 100$ km).

fragmentation delta-velocity distribution, colored by the capture metric in Eq. (7). In this case, 60/724 fragments are captured by the gravitational well at 75°E—of these, 57 are ejected at fragmentation delta-velocities less than 100 m/s, and three at fragmentation delta-velocities larger than 100 m/s, indicating that the direction of the fragmentation delta-velocity vector for these high-speed fragments is opposite to the direction of the parent body's velocity vector. Furthermore, Fig. 3(b) illustrates that area-to-mass ratios consistent with the definition of the high area-to-mass ratio (HAMR) objects observed in the GEO regime[10] are sampled via the NASA Standard Breakup Model in this study, underlying the importance of including SRP in the force model, which is a dominating perturbation for this class of objects [10].

The five-year congestion forecasts for simulated R/B explosions occurring at 45°E, 60°E, and at the Eastern gravitational well at 75°E are illustrated in Fig. 4 for a torus minor radius of $\tilde{r} = 100$ km. Note that 54, 60, and 69 of the 724 generated fragments are captured by the Eastern gravitational well in each case, respectively, and begin librating around this critical longitude. As a consequence, bi-annual "debris storms"—dramatic increases in localized congestion—occur at the longitudinal extents of the parent body's libration motion. This result is predicted by Eq. (9), which states that $\psi_0 = \psi_m$ if $\dot{\psi}_0 = 0$, that is, the amplitude of the libration is equivalent to the initial deviation from the gravitational well inasmuch as $a = r_{\mathrm{GEO}}$ at the explosion epoch. The congestion forecasts in Fig. 4 illustrate that the resulting oscillations in longitude exhibited by the captured fragments synchronize in approximately one-year intervals at the libration amplitude of the parent R/B over the five-year prediction span. Therefore, this is critical knowledge not only for satellite operators with assets in longitude slots near the explosion longitude λ_0, but also for those with assets in longitude slots $2\psi_m$ away from λ_0 in the direction of the gravitational well. Note that the resulting background noise from the drifting fragments not captured by the gravitational well exhibits a yearly "banding"

[10] HAMR objects are defined as having area-to-mass ratios from 0.1 to 20 m^2/kg and above, and are widely studied in the literature—see Kelecy et al. [18] and Früh and Jah [10].

phenomenon driven by once-yearly oscillations in the eccentricity magnitude induced by SRP, the effects of which are more pronounced as a consequence of higher area-to-mass ratios (cf. Fig. 3(b)) [5,17].

Fig. 5 provides a zoomed-in, one-year view of the five-year congestion forecast shown in Fig. 4(b). Curving traces of the fragments captured by the gravitational well are clearly visible, in addition to the linear traces of the higher-energy fragments that evade capture and begin circulating around the GEO ring, with eastward drift for semi-major axes below the GEO altitude, and westward drift for semi-major axes above GEO [2]. Fig. 6(a) shows the 60°E case in Fig. 4(b) propagated for 30 years to illustrate localized congestion trends occurring over this longer time scale. Longitudinal focusing, although prominent for the first five years, begins to diffuse from 5 to 10 years, leading to a lull in localized

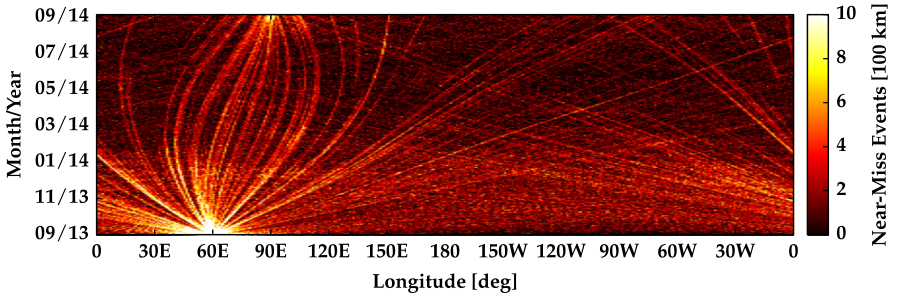

Fig. 5. Longitude-dependent congestion from simulated R/B explosion at 60°E (1 year).

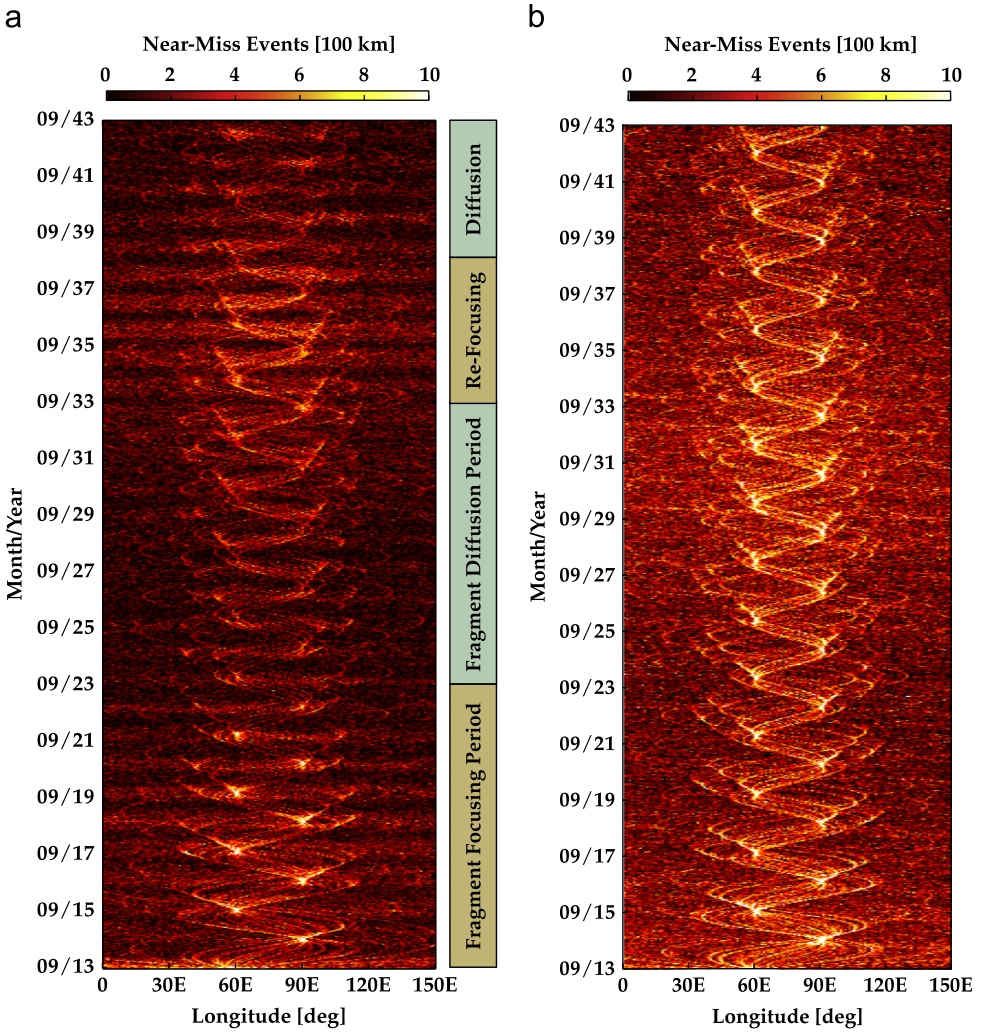

Fig. 6. Longitude-dependent congestion from simulated R/B explosion at 60°E (30 years). (a) Propagation under 4 × 4 gravitation, luni-solar perturbations, and SRP. (b) Propagation under 4 × 4 gravity only.

congestion levels from 10 to 20 years. From 20 to 25 years, the librating fragments begin refocusing into a characteristic oscillatory pattern, but the intensity of these "residual" debris storms is beneath that observed in the first five years following the explosion. After 25 years past fragmentation, the librating fragments once again diffuse.

Analysis of simulation results indicates that the mechanism for this long-term focusing, diffusion, and re-focusing phenomenon is a combination of long-period luni-solar effects and SRP-induced eccentricity variations prevalent for GEO. If these perturbations are removed from the force model, such that the 30-year propagation uses 4×4 gravitation only, the localized congestion forecast in Fig. 6(b) appears. In this situation, fragment diffusion and re-focusing is not observed; rather, strong focusing at the libration amplitude persists throughout the entire 30-year simulation. This result emphasizes a conclusion of Hansen and Sorge [11] that luni-solar and SRP perturbations are critical for analyzing fragmentation events at GEO over durations longer than one year.

Fig. 7 illustrates that similar focusing effects can occur for fragments captured by the Western gravitational well. For simulated R/B explosions at 75°W, 90°W, and at the Western gravitational well at 105°W, 58, 67, and 66 of the 724 ejected fragments are captured in each case, respectively. Although the number of captured fragments in each case is similar to the number captured in the Eastern well simulations illustrated in Fig. 4, the intensities of the fragment focusing events are not as strong as the equivalent Eastern well cases, e.g., for $\psi_0 = 30°$, cf. Figs. 4(a) and 7(a). For completeness, Fig. 8 illustrates the five-year congestion resulting from an explosion at 165°E, a well-known unstable equilibrium longitude located halfway between the stable gravitational wells. In this situation, none of the 724 ejected fragments are captured by either gravitational well via the metric in Eq. (7); however, curvilinear traces in Fig. 8 indicate that several fragments begin oscillating about both the gravitational wells, behavior indicative of L3 class objects (recall Table 1).

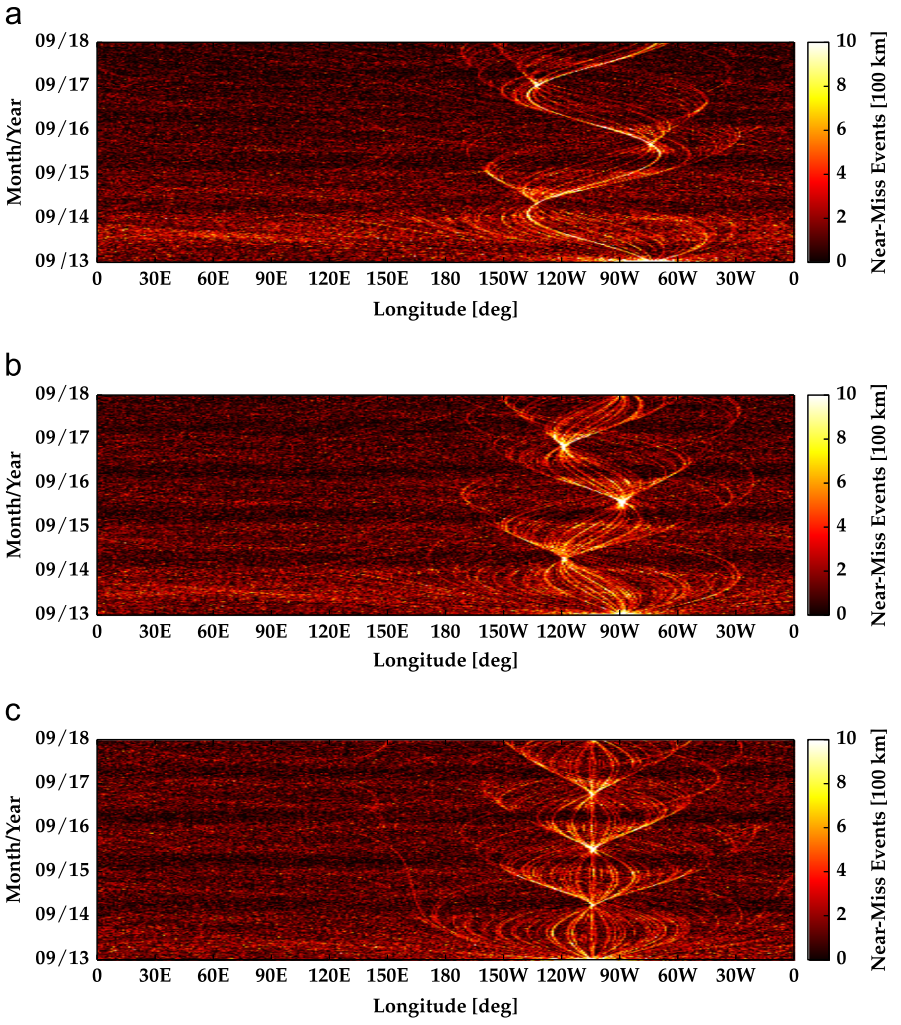

Fig. 7. Longitude-dependent congestion from simulated R/B explosions by Western well. (a) Five-year congestion forecast for simulated explosion at 75°W ($\tilde{r} = 100$ km). (b) Five-year congestion forecast for simulated explosion at 90°W ($\tilde{r} = 100$ km). (c) Five-year congestion forecast for simulated explosion at 105°W ($\tilde{r} = 100$ km).

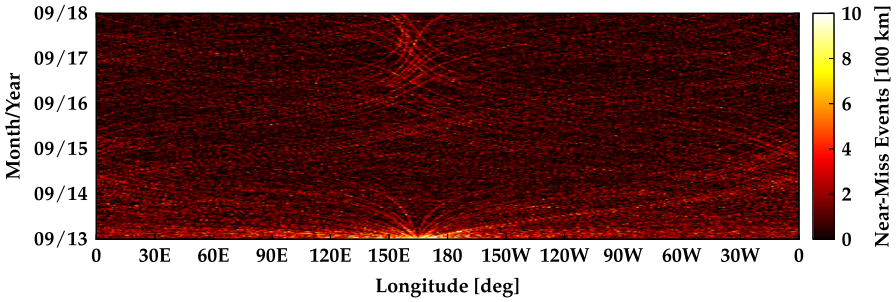

Fig. 8. Longitude-dependent congestion from simulated R/B explosion at 165°E.

4.3. Accuracy of harmonic oscillator model

It is interesting to assess if the harmonic oscillator model in Eqs. (11) and (12) can sufficiently approximate the longitudinal focusing illustrated in the five-year congestion forecasts in Fig. 4. Fragment focusing at the longitudinal extents appears predictable both in longitude and in time, such that a first-order model for forecasting these debris storms with minimal knowledge of the fragment distribution is desirable. If the semi-major axes a_i for the resulting fragment orbits in the aftermath of a fragmentation can be reasonably estimated, $\dot{\psi}_{0,i}$ is a known initial condition, and Eqs. (9) and (10) can be harnessed to compute the amplitude and period of libration for fragments captured via Eq. (7). Longitude histories for these fragments are thus predicted analytically as a function of elapsed time using the model in Eqs. (11) and (12), and overlaid to forecast (to first-order) when and where librating fragment focusing will occur following a fragmentation at GEO.

Fig. 9 illustrates the accuracy of this harmonic oscillator model, showing comparisons between the analytic longitude histories predicted using the model in Fig. 9(a), simulated longitude histories under the $J_{2,2}$ harmonic alone in Fig. 9(b), and simulated longitude histories under 4×4 gravitation, luni-solar perturbations, and SRP in Fig. 9(c). As anticipated, the harmonic oscillator approximation agrees well with the simulated longitudes under $J_{2,2}$ only, as this was the assumption made in the derivation of Eqs. (9) and (10). When compared against "truth" longitude histories for the 60 librating fragments in Fig. 9(c), however, discrepancies exist not in the longitudinal location of the fragment focusing events, but in the times at which these focusing events occur. As errors in timing accumulate with time elapsed since fragmentation, this harmonic oscillator model should only be considered for short-term, 1–2 year predictions. Following this time span, dominating perturbations in the GEO environment that are not accounted for in the harmonic oscillator approximation begin influencing the libration motion of the fragments, and this $J_{2,2}$−only approximation diverges.

4.4. Rocket body collisions over gravitational wells

Finally, it is of interest to investigate the longitude-dependent congestion signature of collision events in the GEO ring. Hansen and Sorge [11] indicate that since orbital velocities are lower for GEO—and objects are orbiting in the same direction—relative velocities are generally more benign for GEO than for LEO. Thus, according to Eq. (5), although fewer fragments will be generated for a collision event at GEO than for an equivalent event at LEO, peak risk potential increases as a result of a smaller-mean fragmentation delta-velocity distribution [11]. For this study, three collisions near the Eastern gravitational well are simulated: (a) collision due to inclination difference Δi, (b) collision due to eccentricity difference Δe, and (c) collision between a GEO object and one in geostationary transfer orbit (GTO). For all scenarios, two 2000 kg upper stages are assumed to collide at 60°E, using the initial conditions of the "target" R/B implemented for the explosion cases shown earlier in Section 4.2. Simulation results are given in Table 2, and the five-year localized congestion forecasts for each collision scenario are provided in Fig. 10.

The first two simulated collisions are non-catastrophic according to the specific energy defined in Eq. (6), and a smaller proportion of fragments are captured by the gravitational well for both of these cases than for the 60°E explosion case (6.5% and 5.7% are captured for the inclination and eccentricity difference collision scenarios, respectively, compared to the 8.3% captured in the explosion case). This is largely a consequence of the fragmentation velocity distribution in the NASA Standard Breakup Model, which defines a higher mean Δv for collision events than for explosion events [16]. In the third simulated collision event—defined as catastrophic according to Eq. (6)—a mere 2.6% of the staggering 8439 fragments larger than 5 cm in diameter are captured by the gravitational well at 75°E.

Fig. 10 shows that the localized congestion forecasts generated by collision events qualitatively appear to be very similar to the macroscopic trends exhibited by explosion events, even though two separate fragment clouds exist in the former, and only a single cloud of ejecta is generated in the latter. The significant increase in the number of near-miss events at 100 km for the GEO-GTO collision in Fig. 10(c) is a consequence of the large number of fragments ejected in this catastrophic collision only. Longitudinal bunching at the libration amplitude of the target R/B is still observed with similar periodicity in all three collision scenarios, although localized congestion during a bunching event in Fig. 10(c) is a factor of four times more intense than for the inclination and eccentricity difference scenarios in Fig. 10(a) and (b). These results indicate that the longitude-dependent effects of explosion and collision events in the GEO regime are equivalent in characteristic, and differ solely by the number of fragments that are captured by the gravitational well in each scenario (cf. Figs. 4(b) and 10).

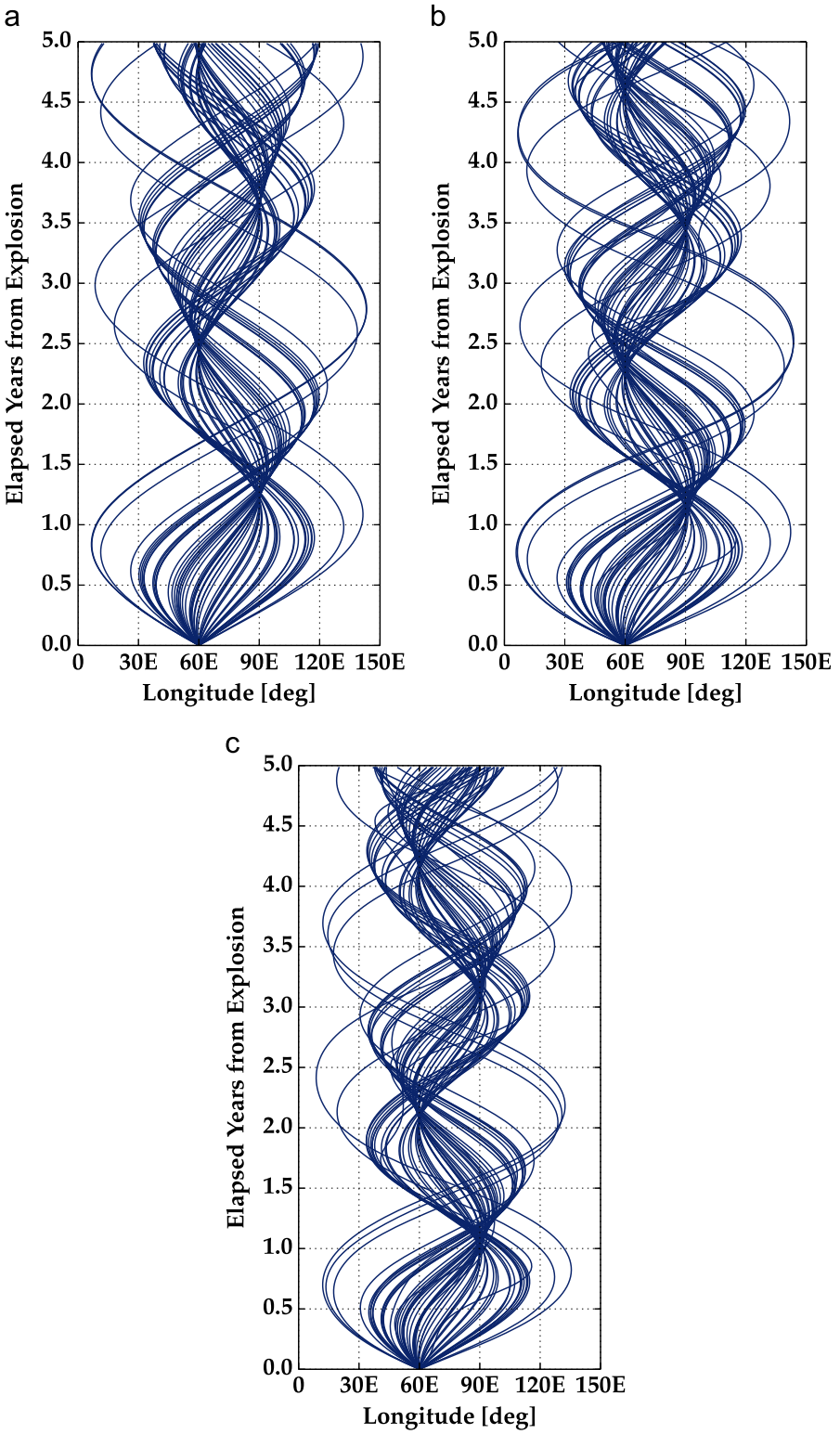

Fig. 9. Accuracy of harmonic oscillator model for predicting longitudes of librating fragments. (a) Harmonic oscillator model. (b) Longitude histories ($J_{2,2}$ only). (c) Longitude histories (4×4 gravitation, luni-solar perturbations, and SRP).

Table 2
Simulation results for three collision scenarios between two 2000 kg upper stages at 60°E, where NC and C denote non-catastrophic and catastrophic collisions, respectively.

Collision scenario description	Collision speed	N_f (Capt.)
Inclination difference $\Delta i = 2.0^\circ$	0.107 km/s (NC)	941 (61)
Eccentricity difference $\Delta e = 0.05$	0.157 km/s (NC)	1251 (71)
At apogee of 200 km × 35,744 km GTO	1.479 km/s (C)	8439 (218)

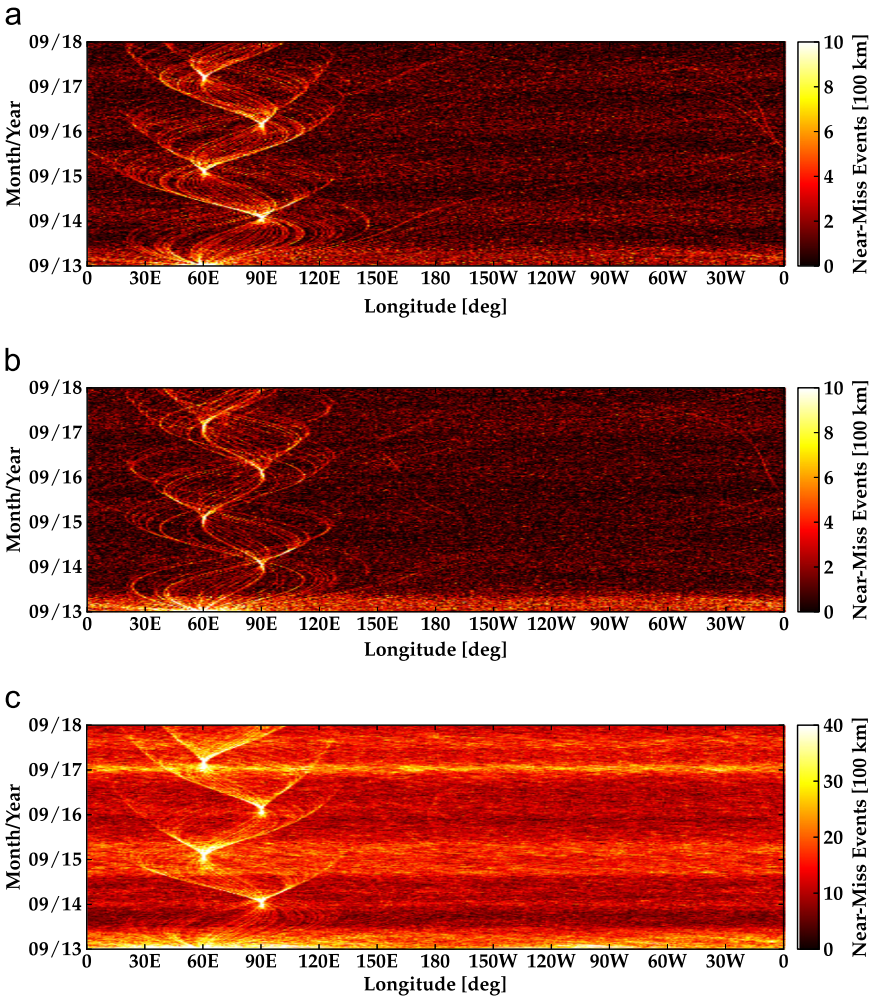

Fig. 10. Longitude-dependent congestion from simulated R/B collisions by Eastern well. (a) Five-year congestion forecast for simulated collision at 60°E (inclination difference). (b) Five-year congestion forecast for simulated collision at 60°E (eccentricity difference). (c) Five-year congestion forecast for simulated collision at 60°E (GEO-GTO apogee collision).

5. Conclusions

The effect of on-orbit fragmentation events on longitude-dependent debris congestion in the GEO regime is investigated by simulating explosions and collisions of uncontrolled rocket bodies in various orbit configurations, including libration about one or both of the critical E/W stable longitudes at the GEO altitude. Applying the NASA Standard Breakup Model in tandem with the torus intersection metric and a parallel propagation routine, both short- and long-term localized congestion patterns are rapidly forecasted to investigate how strongly the severity of GEO fragmentation events depends upon the longitude of the parent body at the epoch of fragmentation. Simulation results indicate that on-orbit GEO fragmentations in the vicinity of one of the critical gravitational wells spawn bi-annual debris storms at the longitudinal extents of the parent body's libration motion. Provided the semi-major axis distribution for a GEO fragmentation can be reasonably estimated using tracking data, longitudes and times at which dramatic increases in congestion

will occur can be predicted to first-order, using the presented harmonic oscillator formulation for time scales of less than five elapsed years.

For all fragmentation scenarios, the level of existing TLE background noise is achieved or surpassed strictly during observed longitudinal focusing events. The intensity of these longitude-dependent debris storms is proportional to the number of particles captured by the nearest gravitational well, however, and thus could readily overtake background congestion levels if higher-energy collisions are considered (as in the scenario of the GTO apogee collision), or if fragment diameters smaller than 5 cm are included. Ultimately, this study highlights the importance of energy passivation at end-of-life—satellites and upper stages that are not appropriately prepared for disposal during decommissioning operations are prone to fragmenting and generating a debris cloud that threatens severe consequences for operational assets in the GEO regime.

Acknowledgments

The authors would like to acknowledge the U.S. Department of Defense and the National Defense Science and Engineering Graduate Fellowship (NDSEG), the program that provided funding for this research. The authors furthermore acknowledge Brandon Jones and the TurboProp software [12], from which the integration routines employed in this research were obtained.

References

[1] R.R. Allan, Perturbations of a geostationary satellite by the longitude-dependent terms in the earth's gravitational field, Planetary Space Sci. 11 (August) (1963) 1325–1334.
[2] P.V. Anderson, H. Schaub, Local orbital debris flux study in the geostationary ring, Adv. Space Res. 51 (June (12)) (2013) 2195–2206.
[3] P.V. Anderson, H. Schaub, Local debris congestion in the geosynchronous environment with population augmentation, Acta Astronaut. 94 (February (2)) (2014) 619–628.
[4] M.M. Berry, L.M. Healy, Implementation of Gauss–Jackson integration for orbit propagation, J. Astronaut. Sci. 52 (3 (July–September)) (2004) 331–357.
[5] C.-C. Chao, Applied Orbit Perturbation and Maintenance, The Aerospace Press, El Segundo, CA, 2005.
[6] V.A. Chobotov (Ed.), Orbital Mechanics, 3rd ed. American Institute of Aeronautics and Astronautics, Inc., Reston, VA, 2002.
[7] P. Chrystal, D. McKnight, P. Meredith, Space Debris: on Collision Course for Insurers? Technical Report, Swiss Reinsurance Company Ltd., 2011.
[8] H. Curtis, Orbital Mechanics for Engineering Students, Elsevier Butterworth-Heinemann, Burlington, MA, 2005.
[9] T. Flohrer, Classification of Geosynchronous Objects: Issue 15, Technical Report 1, European Space Operations Centre, February 2013.
[10] C. Früh, M. Jah, Coupled orbit-attitude motion of high area-to-mass ratio (hamr) objects including efficient self-shadowing, Acta Astronaut. 95 (February–March) (2014) 227–241.
[11] B.W. Hansen, M.E. Sorge, Summarizing the general effects of breakup debris in geo, in: Proceedings of the 2013 AAS/AIAA Astrodynamics Specialist Conference. No. 13-844, August 2013.
[12] K. Hill, B.A. Jones, TurboProp Version 4.0. Colorado Center for Astrodynamics Research, University of Colorado at Boulder, May 2009.
[13] F.R. Hoots, R.L. Roehrich, December 1980. Spacetrack Report No. 3: Models for Propagation of Norad Element Sets, Technical Report, Office of Astrodynamics, Aerospace Defense Center.
[14] R. Jehn, V. Agapov, C. Hernandez, The situation in the geostationary ring, Adv. Space Res. 35 (2005) 1318–1327.
[15] N. Johnson, Protecting the geo environment: policies and practices, Space Policy 15 (1999) 127–135.
[16] N.L. Johnson, P.H. Krisko, J.-C. Liou, P.D. Anz-Meador, Nasa's new breakup model of evolve 4.0, Adv. Space Res. 28 (9) (2001) 1377–1384.
[17] S. Jones, Negating the yearly eccentricity magnitude variation of super-synchronous disposal orbits due to solar radiation pressure (Master's thesis), University of Colorado at Boulder, 2013.
[18] T. Kelecy, M. Jah, J. Baldwin, J. Stauch, High area-to-mass ratio object population assessment from data/track association, Acta Astronaut. 96 (March–April) (2014) 166–174.
[19] H. Klinkrad, Space Debris: Models and Risk Analysis, Praxis Publishing, Chichester, United Kingdom, 2006.
[20] K. Luu, C. Sabol, Effects of Perturbations on Space Debris in Supersynchronous Storage Orbits, Technical Report, Air Force Research Laboratory, October 1998.
[21] D.S. McKnight, Simulation of on-orbit satellite fragmentations (Ph.D. thesis), University of Colorado at Boulder, 1986.
[22] D.S. McKnight, F.R. Di Pentino, New insights on the orbital debris collision hazard at geo, Acta Astronaut. 85 (2013) 73–82.
[23] D.S. McKnight, F.R. Di Pentino, P. Dingman, Semi-empirical satellite anomalies analysis highlighting contributions from the fengyun-1c, in: Proceedings of the 64th International Astronautical Congress, 2013.
[24] O. Montenbruck, E. Gill, Satellite Orbits: Models, Methods, Applications, Springer, Heidelberg, Germany, 2000.
[25] D. Oltrogge, D. Finkleman, Consequences of debris events in geosynchronous orbit, in: Proceedings of the 2008 AIAA/AAS Astrodynamics Specialist Conference and Exhibit, No. 2008-7375, August 2008.
[26] T. Schildknecht, R. Musci, M. Ploner, G. Beutler, W. Flury, J. Kuusela, J. de Leon Cruz, L. de Fatima Dominguez Palmero, Optical observations of space debris in geo and in highly-eccentric orbits, Adv. Space Res. 34 (2004) 901–911.
[27] T. Schildknecht, M. Ploner, U. Hugentobler, The search for debris in geo, Adv. Space Res. 28 (9) (2001) 1291–1299.
[28] USNO, UKHO, The Astronomical Almanac for the Year 2013, U. S. Nautical Almanac Office with Her Majesty's Nautical Almanac Office, 2013.
[29] D. Vallado, Fundamentals of Astrodynamics and Applications, 3rd ed. Microcosm Press, Hawthorne, CA, 2007.
[30] D.A. Vallado, P. Crawford, R. Hujsak, T.S. Kelso, Revisiting Spacetrack Report no. 3: Revision 2, in: Proceedings of the 2006 AIAA/AAS Astrodynamics Specialist Conference, August 2006.
[31] P. Wegener, J. Bendisch, H. Krag, M. Oswald, S. Stabroth, Population evolution in the geo vicinity, Adv. Space Res. 34 (2004) 1171–1176.
[32] T. Yasaka, N. Ishii, Breakup in geostationary orbit: a possible creation of a debris ring, Acta Astronaut. 26 (7) (1992) 523–530.